Precipitation in Nb-Stabilized Ferritic Stainless Steel Investigated with *in-situ* and *ex-situ* Transmission Electron Microscopy

A. MALFLIET, F. MOMPIOU, F. CHASSAGNE, J.-D. MITHIEUX, B. BLANPAIN, and P. WOLLANTS

A Nb-stabilized Fe-15Cr-0.45Nb-0.010C-0.015N ferritic stainless steel is studied with transmission electron microscopy (TEM) to investigate the morphology and kinetics of precipitation. $Nb_x(C,N)_y$ and MnS precipitates are present in the steel in the initial condition. *Ex-situ* TEM analysis is performed on samples heat treated at 973 K, 1073 K, 1173 K, and 1273 K (700 °C, 800 °C, 900 °C, and 1000 °C). Within this temperature range, both Fe_2Nb and $Fe_3Nb_3X_x$ (with X = C or N) precipitates form. Fe_2Nb is observed at 1073 K (800 °C). $Fe_3Nb_3X_x$ precipitates form at the grain boundaries between 973 K and 1273 K (700 °C and 1000 °C). Up to at least 1173 K (900 °C) their fraction increases with time and temperature, but at 1273 K (1000 °C) they lose stability with respect to $Nb_x(C,N)_y$. With *in-situ* TEM, no phase transition is observed between room temperature and 1243 K (970 °C). At 1243 K (970 °C) the precipitation of $Fe_3Nb_3X_x$ is observed in the neighborhood of a dissolving $Nb_2(C,N)$ precipitate. For sections of grain boundaries where no $Nb_x(C,N)_y$ precipitates are present, $Fe_3Nb_3X_x$ does not form. It is concluded that the precipitation of $Fe_3Nb_3X_x$ is directly related to the dissolution of $Nb_2(C,N)$ through the redistribution of C or N.

DOI: 10.1007/s11661-011-0745-5

I. INTRODUCTION

IN the last decade, the steel market for automotive exhaust systems was characterized by an increased use of ferritic stainless steel at the expense of the austenitic grades. Although basic austenitic stainless steel grades offer better mechanical properties at high temperatures than similar ferritic grades, the high and fluctuating Ni prices are a major drawback of the former grades. This economical disadvantage has favored the development of ferritic grades with similar high-temperature properties as the austenitic grades, for example, Nb stabilized ferritic stainless steel.

Nb increases the high-temperature strength of the steel by solid solution hardening.[1–3] The formation of Nb containing precipitates is reported to affect the strength and the creep resistance.[2,4] As the mechanical properties change with the distribution, size, and nature of the precipitates, it is desirable to know the stability, formation kinetics, and morphology of the different precipitates in Nb-stabilized ferritic stainless steel grades.

In general, in a Fe-Cr-Nb-C-N steel, three kinds of Nb precipitates are observed, i.e. hexagonal Fe_2Nb, face-centered-cubic Nb(C,N), and a cubic Fe_3Nb_3C phase with prototype Fe_3W_3C. According to the work of Sim *et al.*,[5] Nb(C,N) and Fe_2Nb precipitates coexist in an industrial Fe-15Cr-0.38Nb-0.01C steel after 2 hours heat treatment at 973 K (700 °C). After 1000 hours, Fe_3Nb_3C precipitates are observed. A linear relationship between proof strength and Nb content in solid solution was observed. It is stated that the precipitation of Nb(C,N) decreases slowly the high-temperature strength, whereas the faster coarsening of Fe_2Nb precipitates abruptly decreases this strength. Fujita *et al.*[6] determined the solubility product of the Fe_3Nb_3C phase in different Fe-Cr-Nb-C-N ferritic stainless steel grades between 973 K and 1273 K (700 °C and 1000 °C). Their results indicate that the amount of Fe_3Nb_3C increases with ageing time and temperature and that Cr enhances the formation of this Fe_3Nb_3C phase. Also, according to Fujita *et al.*,[3] the reduction in proof strength at 1173 K (900 °C) of a steel with 0.5 wt pct Nb after 500 hours at 1173 K (900 °C) with respect to the steel in its initial condition is explained through the formation and coarsening of Fe_3Nb_3C precipitates, resulting in a loss of Nb in solid solution. Chassagne *et al.*[4] observed precipitates with similar crystallography and stoichiometry as the Fe_3Nb_3C phase in an industrial Nb-stabilized ferritic stainless steel; however, because there was no clear presence of light elements in these precipitates, it was

---

A. MALFLIET, PhD, B. BLANPAIN and P. WOLLANTS, Professors, are with the Department of Metallurgy and Materials Engineering, Katholicke Universiteit Leuven, 3001 Heverlee, Belgium. Contact e-mail: annelies.malfliet@mtm.kuleuven.be F. MOMPIOU, PhD, is with CEMES, Centre d'Elaboration des Matériaux et d'Etude Structurale, 31055 Toulouse, Cedex 4, France. F. CHASSAGNE, Senior Metallurgist, and J.-D. MITHIEUX, Research Engineer in Metallurgy, are with APERAM Isbergues Research Centre (formerly ArcelorMittal Isbergues Research Centre), 62330 Isbergues, France.

Manuscript submitted November 16, 2010.

referred to as Fe_2Nb_3. Their results indicate that depending on temperature and steel composition, either Fe_2Nb or Fe_2Nb_3 precipitates form, with Fe_2Nb_3 being more stable at higher temperature. By performing sag tests, Chassagne *et al.* were able to identify the influence of these precipitates on the creep resistance of the steel.

It should be noted that in these studies where Fe_3Nb_3C precipitates are observed,[1,3,5,6] the actual C concentration is not determined. In compounds of the filled Ti_2Ni type, to which the Fe_3Nb_3C phase belongs, different light elements in different concentrations can stabilize the same metallic compound. For example, both Fe_3Nb_3N and Fe_6Nb_6O are known to exist.[7,8] Therefore, it is not excluded that in a Fe-Cr-Nb-C-N ferritic stainless steel, N could as well be present in these assumed Fe_3Nb_3C precipitates. In this study, the general formula $Fe_3Nb_3X_x$ will be used, regardless of the nature of the stabilizing light element.

This work aims to complement the studies of Sim[5] and Fujita[6] with morphology and kinetic data of the $Fe_3Nb_3X_x$ precipitates from *ex-situ* and *in-situ* transmission electron microscopy (TEM) observations. Data on their formation and growth as a function of time and temperature are valuable information with respect to the mechanical properties of the steel. The same ferritic stainless steel as that in the work of Chassagne[4] containing initial $Nb_x(C,N)_y$ precipitates is selected. With the *in-situ* TEM experiments, the effect of the dissolution of $Nb_x(C,N)_y$ precipitates on the formation of $Fe_3Nb_3X_x$ precipitates can be directly investigated.

II. MATERIALS AND METHODS

Table I shows the chemical composition of the ferritic stainless steel used in this investigation. This steel was subjected to the classical production process for sheet, i.e., casting, hot and cold rolling to the desired thickness, and annealing at 1323 K (1050 °C) for recrystallization. The precipitation behavior of this alloy is analyzed by *in-situ* TEM and *ex-situ* TEM. The sample preparation and analysis conditions for both techniques are described in the Sections II–A and II–B. Figure 1 illustrates the sample preparation.

A. *Ex-situ TEM*

Bulk samples ($30 \times 10 \times 1.5 mm^3$) of the alloy in Table I are heated to 973 K, 1073 K, 1173 K, and 1273 K (700 °C, 800 °C, 900 °C, and 1000 °C) for 3, 10, 30, and 90 minutes. For TEM investigation of the precipitates, carbon extraction replicas are prepared. After grinding and polishing, the samples are etched for 4 minutes in a picric solution (20 g/L picric acid, 50 mL/L HCl, and diluted with ethanol) followed by deposition of a carbon nanolayer. This layer, containing the precipitates, is removed from the sample by dissolving the steel matrix in the same picric solution. The carbon replica is positioned on a copper grid before inserting it in the transmission electron microscope.

Table I. Main Composition of the Ferritic Stainless Steel Used in This Investigation; Alloying Elements with a Concentration Less Than 0.05 Wt Pct Are Not Shown the Remaining Is Fe

Element	Cr	Si	Nb	Mn	Ni	C	N	O
Wt pct	14.8	0.576	0.453	0.192	0.112	0.010	0.017	0.003

One sample is heat treated at 1123 K (950 °C) for 500 hours. This sample is prepared by mechanically thinning to less than 100 μm and electropolishing at 20 V in a Struers A2 electrolyte (9 pct water (Aqualab, VWR, Haasrode, Belgium), 73 pct ethanol (Chemlab, Zedelgem, Belgium), 10 pct butoxyethanol (Prolabo, VWR, Haasrode, Belgium) and 8 pct perchloric acid (Chemlab, Zedelgem, Belgium)) using a Tenupol electropolisher. The temperature of the electrolyte is kept between 255 K and 248 K (−18 °C and −25 °C). Bright-field (BF) images, energy dispersive spectrometry (EDS) measurements, and selected area electron diffraction (SAED) patterns are obtained with a PHILIPS* CM200-FEG transmission electron microscope operated at 200 kV. EDS quantification was standardless using a correction factor for thin specimens.

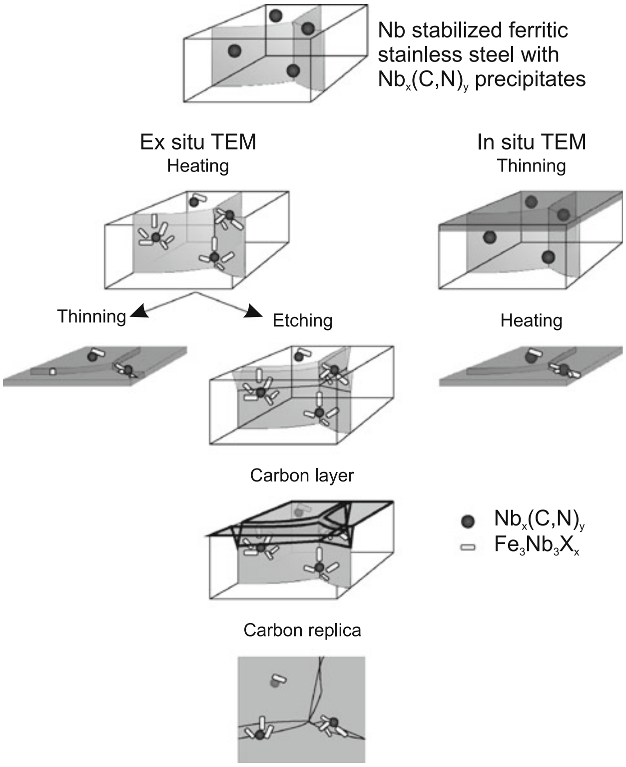

Fig. 1—Sample preparation for *ex-situ* and *in-situ* TEM analysis. Both carbon replicas and electrolytically thinned samples of the heat-treated Nb-stabilized ferritic stainless steel are investigated by *ex-situ* TEM. For the *in-situ* TEM experiment, the sample is heated and observed simultaneously.

---

*PHILIPS is a trademark of FEI Company, Hillsboro, OR.

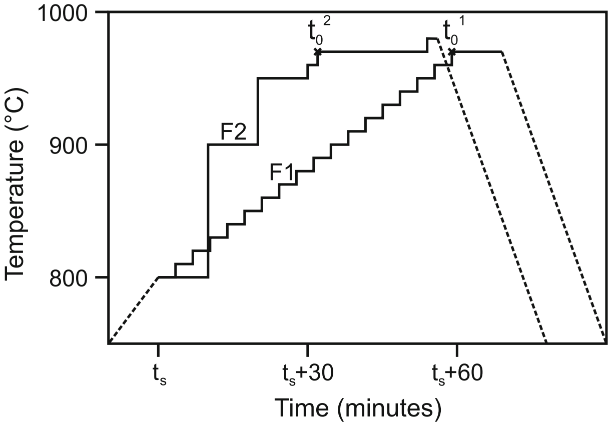

Fig. 2—Heating program of the samples F1 and F2 between 1073 K and 1253 K (800 °C and 980 °C) is the time at which the sample temperature reaches 1073 K (800 °C) and t_0^2 are the times at which the samples reach 1243 K (970 °C).

B. *In-situ TEM*

Thin films are prepared by electrolytically thinning in the same way as the thinned sample for the *ex-situ* TEM experiments. Two samples, F1 and F2 are heated *in-situ* by a Gatan sample holder with heating stage under vacuum in a JEOL** 2010, which is operated at 200 kV. Microstructural changes were observed by means of DVD/HD recording using a Megaview III CCD camera (Soft Imaging Solutions, Münster, Germany). The temperature is measured with a thermocouple in the sample holder at the border with the sample. It is assumed that the temperature difference with the actual observation point is small as the heat conductivity of the steel is relatively large. The heating program with a maximum temperature of 1253 K (980 °C) is shown in Figure 2. TEM observations are done in BF mode, with the magnification set between 40 and 80 k. BF images and SAED patterns are recorded with a Lhesa camera (Lheritier SA, Cergy-Pontoise, France). A PHILIPS CM200-FEG operated at 200 kV is used for postmortem analysis. Standardless EDS analysis of the precipitates is performed using a correction factor for thin specimens.

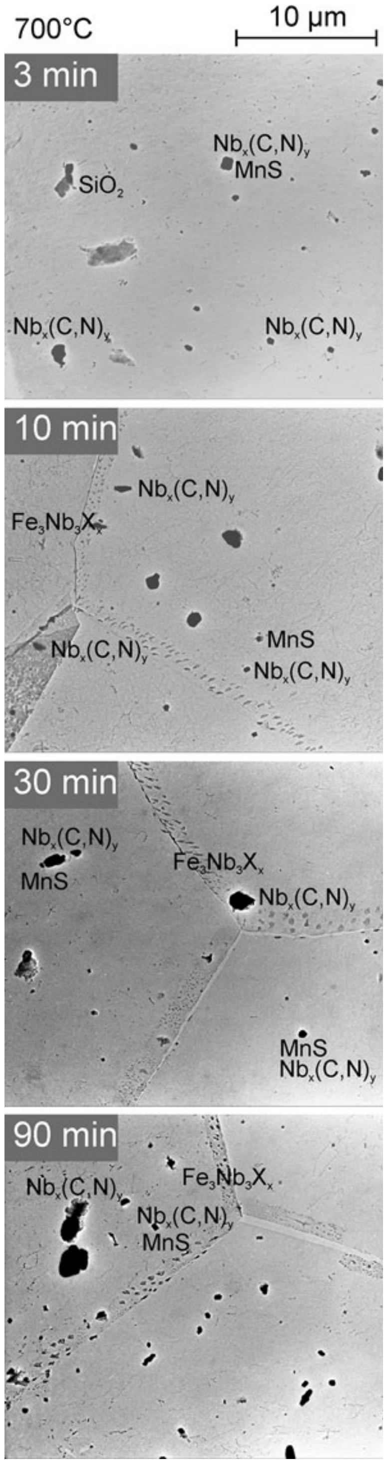

Fig. 3—TEM analysis of the extracted precipitates in Nb-stabilized ferritic stainless steel after heat treatment at 973 K (700 °C) for up to 90 min.

III. RESULTS

A. *Ex-Situ TEM*

The *ex-situ* TEM analysis of the precipitation in the Nb-stabilized ferritic stainless steel using carbon extraction replicas is shown in Figures 3 through 6. These figures show the time and temperature evolution of the different types of precipitates between 973 K and 1273 K (700 °C and 1000 °C) for up to 90 minutes. EDS spectra and SAED patterns are used to characterize the matrix and precipitates (Figures 7 and 8). The Cu peak and, to some extent, the C peak in the EDS spectra are caused by the copper grid and carbon replica, respectively. For the $Fe_3Nb_3X_x$ precipitates, peaks are present at the C and N positions, but the concentration of these elements could not be quantified with EDS. For identification of the precipitates in Figures 3 through 6, EDS was mainly used because it is more efficient to analyze a large

---

**JEOL is a trademark of Japan Electron Optics Ltd, Tokyo.

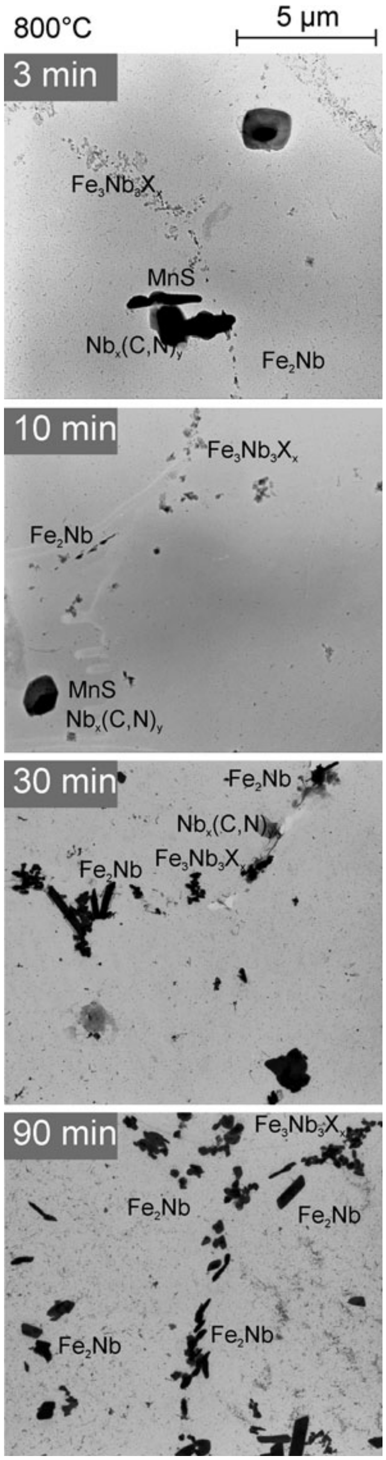

Fig. 4—TEM analysis of the extracted precipitates in Nb-stabilized ferritic stainless steel after heat treatment at 1073 K (800 °C) for up to 90 min.

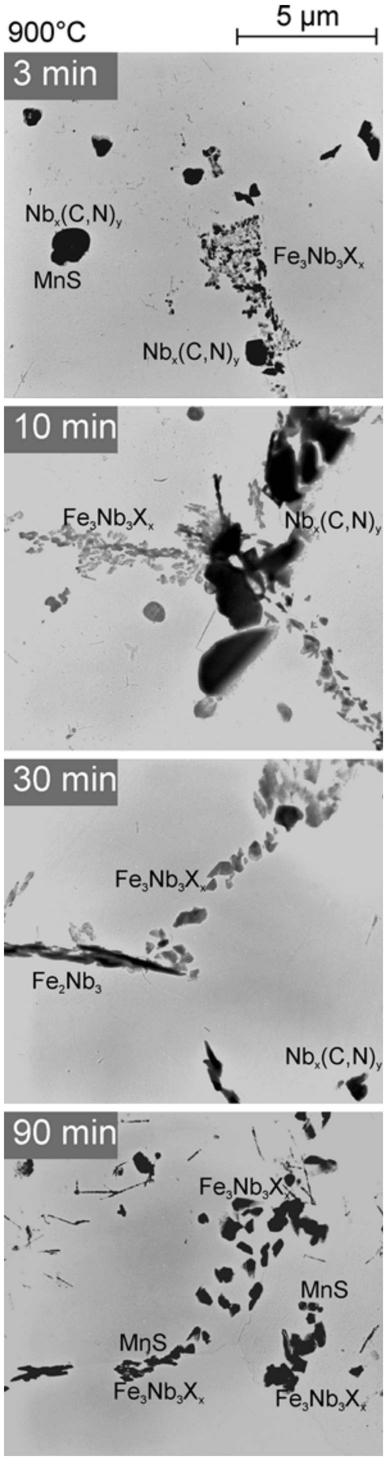

Fig. 5—TEM analysis of the extracted precipitates in Nb-stabilized ferritic stainless steel after heat treatment at 1173 K (900 °C) for up to 90 min.

amount of precipitates than SAED patterns. Through SAED patterns, both Nb(C,N) and Nb_2(C,N) precipitates were identified. As EDS does not allow us to distinguish between them, the general formula $Nb_x(C,N)_y$ is used for both phases. The crystal structure of the $Fe_3Nb_3X_x$ precipitates is identified as a cubic structure with lattice parameter 1.1(4) nm similar to the Fe_3Nb_3C precipitates previously described by Fujita.[6]

After 3 minutes at 973 K (700 °C) the microstructure resembles the original microstructure before heat treatment with mainly $Nb_x(C,N)_y$ and MnS precipitates. After 10 minutes, small $Fe_3Nb_3X_x$ nuclei formed at the

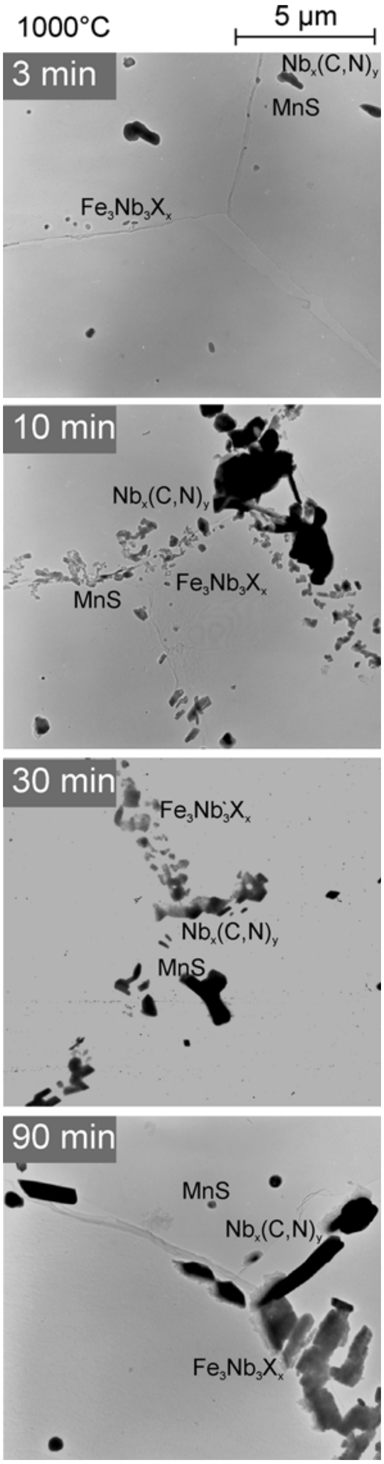

Fig. 6—TEM analysis of the extracted precipitates in Nb-stabilized ferritic stainless steel after heat treatment at 1273 K (1000 °C) for up to 90 min.

grain boundary, while the Nb$_x$(C,N)$_y$ and MnS remain present mainly as intragranular precipitates. This microstructure is maintained up to 90 minutes. By increasing the temperature to 1073 K (800 °C) the Fe$_3$Nb$_3$X$_x$ phase was formed within 3 minutes, but also precipitates of the Fe$_2$Nb phase nucleated. The amount of the Fe$_3$Nb$_3$X$_x$ and Fe$_2$Nb phase appears to increase with heat treatment time at the expense of the Nb$_x$(C,N)$_y$ phase. While the Fe$_3$Nb$_3$X$_x$ phase precipitates only intergranularly, the Fe$_2$Nb phase can be found both on the grain boundaries and in the grains. The Fe$_2$Nb phase is not observed above 1173 K (900 °C). At this temperature, the Fe$_3$Nb$_3$X$_x$phase is the main phase with some Nb$_x$(C,N)$_y$ and MnS. Increasing the temperature to 1273 K (1000 °C) apparently stabilizes again the Nb$_x$(C,N)$_y$ phase at the expense of the Fe$_3$Nb$_3$X$_x$ phase. Large Nb$_x$(C,N)$_y$ precipitates are observed after 90 minutes at this temperature.

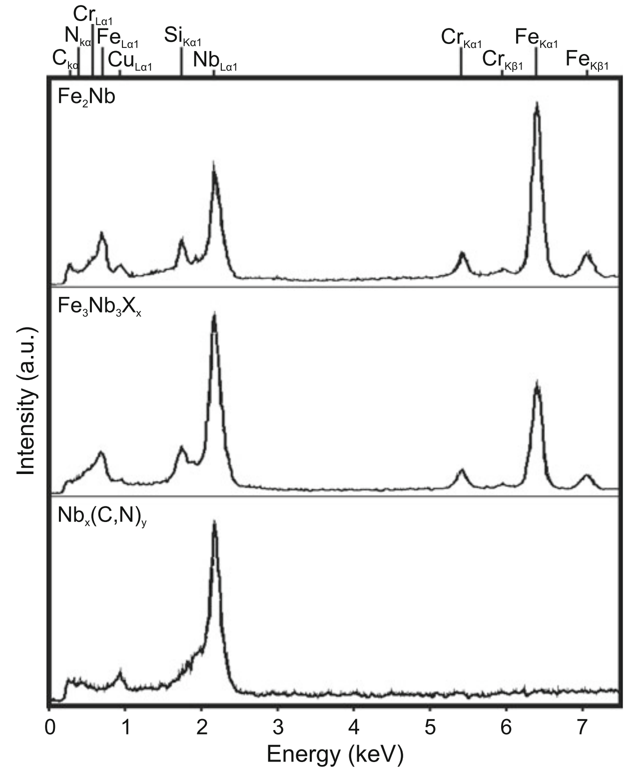

Fig. 7—EDS spectra of the Nb containing precipitates.

The precipitation of the sample heated for 500 hours at 1123 K (950 °C) is shown in Figure 9. At the grain boundaries, the Fe$_3$Nb$_3$X$_x$ precipitates have a diameter of several micrometers.

B. *In-situ TEM*

In samples F1 and F2, a Nb$_x$(C,N)$_y$ precipitate on a grain boundary is selected as an observation spot for the precipitation behavior. SAED investigation of these precipitates indicates that they are both hexagonal Nb$_2$(C,N) phase.

Sample F1 is heated from 1073 K to 1243 K (800 °C to 970 °C) in temperature steps of 10 K according to the heating program in Figure 2. Because no changes in the microstructure of the precipitates were observed below 1123 K (950 °C) the temperature of sample F2 is increased from 1073 K to 1123 K (800 °C to 950 °C) in larger temperature steps. Also, in F2, no changes are observed below 1123 K (950 °C). From 1123 K (950 °C)

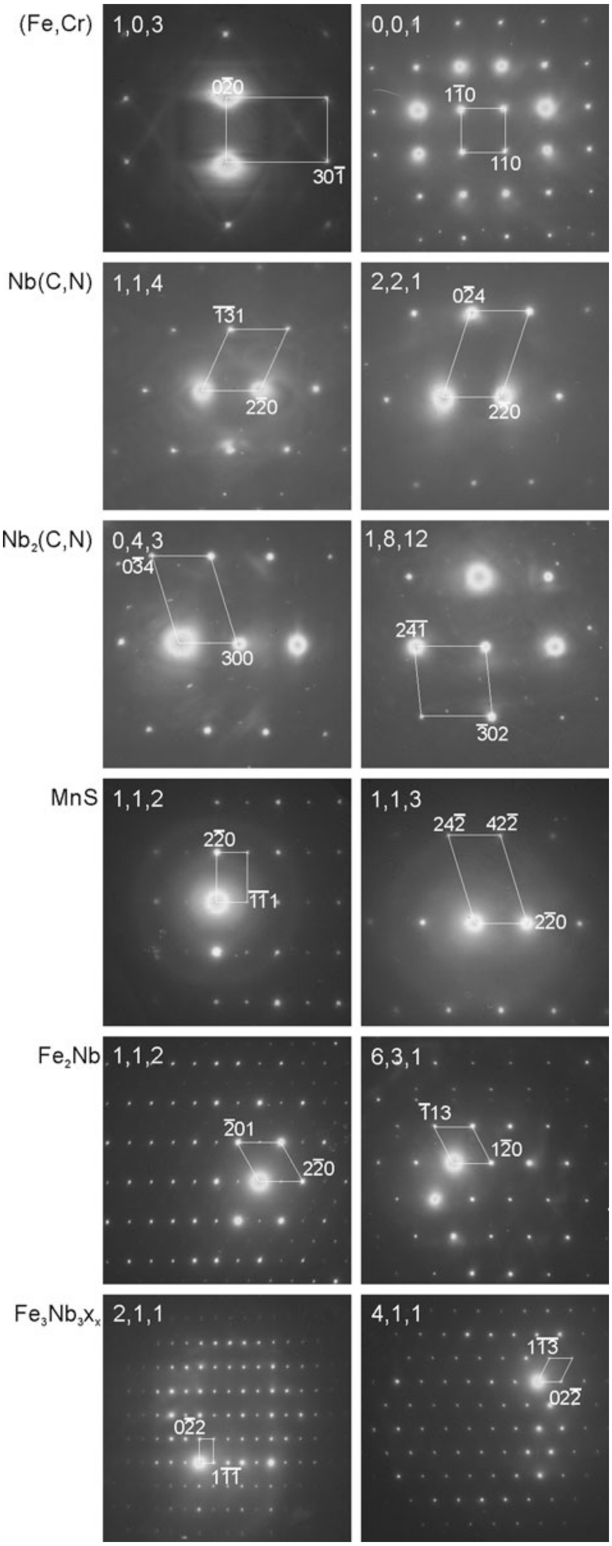

Fig. 8—SAED diffraction patterns of the matrix and precipitates of the Nb-stabilized ferritic stainless steel.

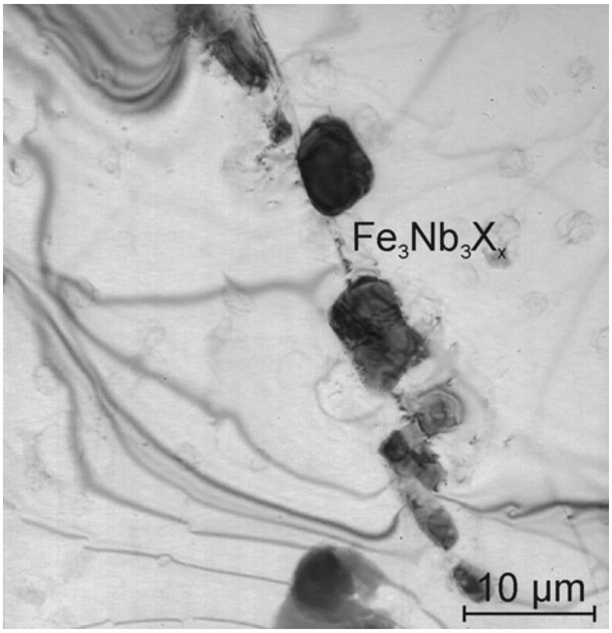

Fig. 9—TEM analysis of the precipitates in a thinned sample of Nb-stabilized ferritic stainless steel, which was subjected to a heat treatment at 1123 K (950 °C) for 500 h.

on, the sample is heated further in temperature steps of 10 K up to 1253 K (980 °C).

In both samples F1 and F2, a change in microstructure is observed at 1243 K (970 °C). The microstructural evolution of sample F1 from the start to the end of the experiment is shown in Figure 10. The time t is the time interval after the time t_0^1 at which the sample reaches 1243 K (970 °C). A new precipitate A nucleates initially at the grain boundary at a distance of about 1.6 μm from the $Nb_2(C,N)$ precipitate. During postmortem analysis of the *in-situ* TEM sample, this precipitate is identified with EDS and SAED to be the $Fe_3Nb_3X_x$ phase. Within the next 10 minutes more precipitates B to F nucleate at the grain boundary in the immediate neighborhood of the initial $Nb_2(C,N)$ precipitate. The sample is then cooled. At the end of the experiment, the $Nb_2(C,N)$ precipitate slightly decreased in volume, but is still clearly present. Most $Fe_3Nb_3X_x$ precipitates have grown preferentially in a direction parallel to the grain boundary plane, leading to an elongated morphology. Further away from the $Nb_2(C,N)$ precipitate, no precipitates are observed.

In sample F2, a clear transition between the initial $Nb_2(C,N)$ and the new precipitates is observed, as shown in Figure 11. The time t indicated in Figure 11 is the time interval after the time t_0^2 at which the sample reaches 1243 K (970 °C). The $Fe_3Nb_3X_x$ precipitates form on to the dissolving $Nb_2(C,N)$ precipitate, but the elongated morphology is less present. Initially, the grain boundary is only slightly curved and touches the $Nb_2(C,N)$ precipitate. During the transition from the $Nb_2(C,N)$ precipitate to the $Fe_3Nb_3X_x$ precipitates, the grain boundary is pinned at the point where the transition takes place, causing the grain boundary next to the precipitates to bow out. After 13 minutes at 1243 K (970 °C) the transition is almost complete. The following 9 minutes the $Fe_3Nb_3X_x$ precipitates grow and the grain boundaries remain pinned by the new precipitates. Finally, the temperature was increased to

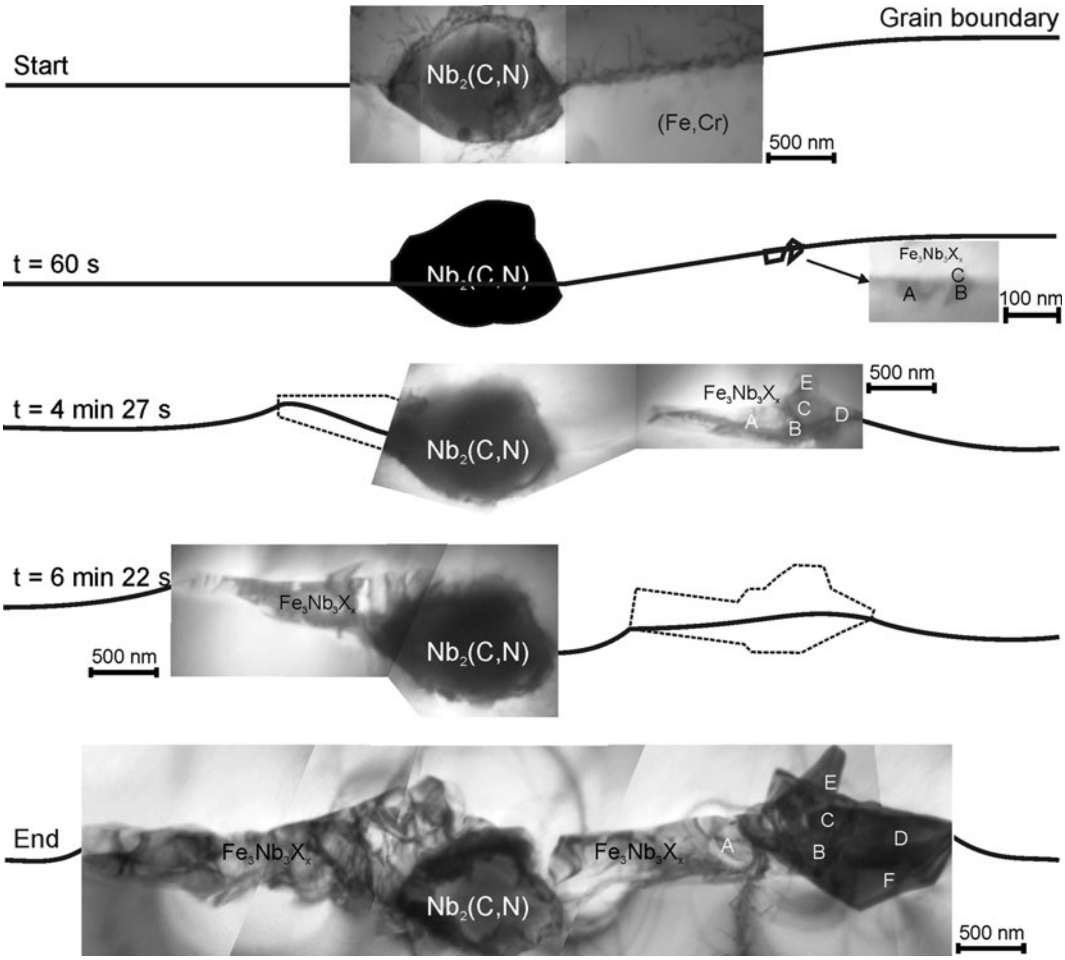

Fig. 10—Nucleation and growth of the precipitates A through F by heating the *in-situ* TEM sample F1 to 1243 K (970 °C) with the indicated time measured from the moment t_0^1. The first precipitate A nucleates on the grain boundary at a distance of ~1.6 μm from the Nb_2(C,N). Within 10 min, also precipitates B through formed, while the Nb_2(C,N) precipitate has slightly decreased in volume.

1253 K (980 °C) to observe the effect of a temperature increase on these grain boundary precipitates. Unfortunately, at these temperatures, the oxidation front at the thin edge of the TEM sample approached the observed precipitates and the experiment had to be stopped.

Postmortem analysis of the investigated samples shows that a morphology similar to the one in Figure 10, where multiple precipitates with elongated morphology are aligned with the grain boundary, is regularly observed.

To analyze the growth of the $Fe_3Nb_3X_x$ precipitates, the small time interval from 60 to 67 seconds in sample F1 is considered where no new precipitates nucleate. Detailed examination of the growth of precipitates A and C in Figure 10, shows that length and width increase almost linearly with time (Figure 12). The growth along the main axis of the precipitates is about ~2.5 to 3.5 nm/s, while perpendicular to this axis, it is ~1.5 nm/s. The growth of these two precipitates between 60 and 600 seconds is shown in Figure 13. For other precipitates, these data could be obtained only during a short time interval or with less accuracy, mainly due to unclear imaging of the phase boundaries and overlapping between precipitates. For most precipitates, the one-dimensional growth rate is still linear in the period of simultaneous nucleation and growth of the $Fe_3Nb_3X_x$ phase, but the initial growth rate of 1.5 to 3.5 nm/s decreases to 0.6 to 1.8 nm/s between 1 and 2 minutes after the first nucleation event (Figure 13). An exception is the length of precipitate A, which can be described better with a logarithmic function. Within 10 minutes, the $Fe_3Nb_3X_x$ precipitates touch the Nb_2(C,N) precipitate at both sides along the grain boundary.

IV. DISCUSSION

The *in-situ* TEM measurements reveal the formation kinetics and morphology of $Fe_3Nb_3X_x$ precipitates with respect to Nb_2(C,N) precipitates located on the grain boundary. This discussion starts with some comments on the difference in samples between *in-situ* TEM and *ex-situ* TEM experiments. Then, the nucleation and growth kinetics of the $Fe_3Nb_3X_x$ precipitates are described based on the *in-situ* observations.

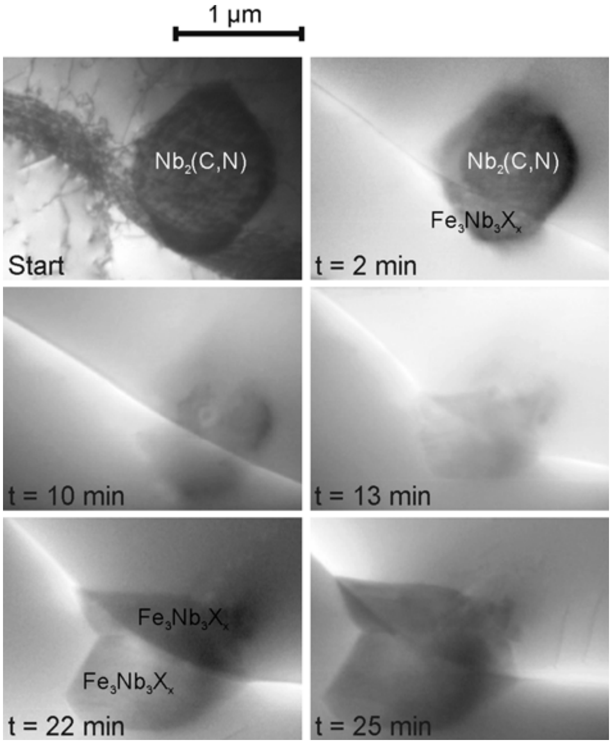

Fig. 11—Continuous transformation from the $Nb_2(C,N)$ precipitate to new precipitates in the sample F2 at 1243 K (970 °C). The first image shows the $Nb_2(C,N)$ at the beginning of the experiment. In the other images, the indicated time is measured from the moment t_0^2 at which the sample reaches 1243 K (970 °C).

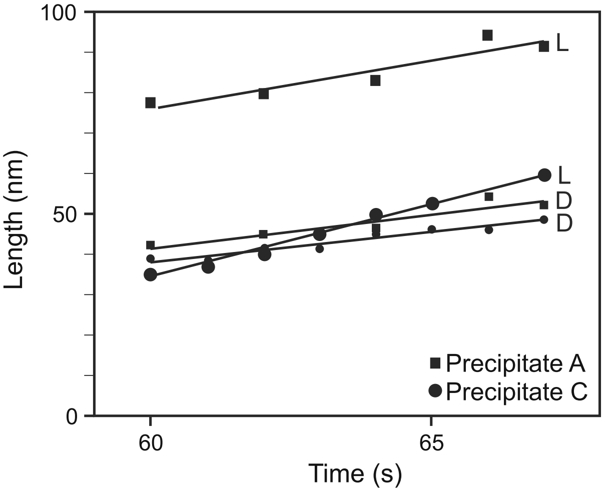

Fig. 12—Growth of the length (*L*) and width (*D*) of the precipitates A and C in the time interval 60 to 67 s after heating the sample F1 to 1243 K (970 °C).

A. *Comparison Between in-situ and ex-situ TEM Experiments*

The effect of the sample preparation for both the *ex-situ* and the *in-situ* experiments is shown in Figure 1. This figure shows the difference in the number and morphology of the precipitates.

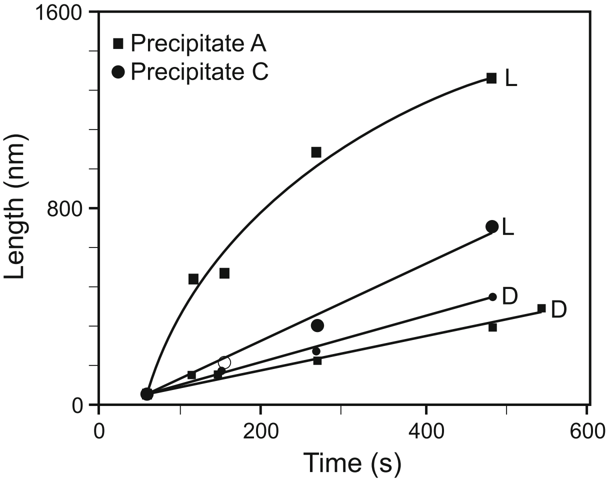

Fig. 13—Growth of the length (*L*) and width (*D*) of the precipitates A and C in the time interval 60 to 540 s after heating the sample F1 to 1243 K (970 °C).

In the *ex-situ* experiments using thinning, variously shaped precipitates can be observed. Their volume fraction is representative for the sample, but it is difficult to determine the exact shape of the precipitates. For instance, when a cylindrical shaped precipitate lies with its long axis perpendicular to the surface plane of the TEM sample, it appears in a thinned sample as a round precipitate.

In the case of carbon extraction replicas, the shape of the precipitates is clearer. As the precipitates are extracted as a whole from the steel, it is easier to distinghuish between a rod-like or a spherical precipitate. Disadvantages of the replica method are that the number of precipitates depends on the degree of etching and that some configurational information is lost. For example, in the case of intergranular precipitates, their location on the grain boundary can still be identified as these precipitates will all lie more or less on a line in the carbon replica. How they were aligned with the grain boundary is lost because the grain boundary is not transferred to the carbon replica.

With *in-situ* TEM experiments, one dimension is very small, leading to a two-dimensional (2-D) morphology that will be different from the one occuring in a bulk sample. When a $Nb_2(C,N)$ precipitate dissolves, thereby releasing Nb, C, and N, grain boundary $Fe_3Nb_3X_x$ precipitates form with their main axis mainly parallel to the plane of the sample and oriented along the grain boundary. On parts of the grain boundaries with no $Nb_2(C,N)$ precipitates, no $Fe_3Nb_3X_x$ appears. This is observed during *in-situ* TEM on grain boundaries close to the observation area but further away from the $Nb_2(C,N)$ precipitate. In addition, postmortem analysis of the *in-situ* TEM samples showed that in the center of a cluster of $Fe_3Nb_3X_x$ precipitates, often a $Nb_2(C,N)$ precipitate can be found. Therefore, this *in-situ* experiment reveals that the formation of the $Fe_3Nb_3X_x$ precipitates is directly related to the presence of $Nb_2(C,N)$ precipitates on the grain boundary. This information is difficult to extract from *ex-situ* TEM, as it is possible to observe $Fe_3Nb_3X_x$ precipitates without a $Nb_2(C,N)$ precipitate when the latter is either already dissolved or not within the thin section of the sample. In addition, with *in-situ* TEM, it is observed that the $Fe_3Nb_3X_x$ phase nucleates initially not next to the $Nb_2(C,N)$ but at some distance from it. From these observations, it can be expected that size and dispersion of the $Nb_2(C,N)$ precipitates affects the final distribution of the $Fe_3Nb_3X_x$ precipitates. This distribution is important for grain boundary pinning. It is observed that the grain boundary remains pinned during the transition from the $Nb_2(C,N)$ to the $Fe_3Nb_3X_x$ precipitates. Although grain boundary pinning in a 2-D system is reported to be stronger than in a three-dimensional (3-D) system,[9] the $Fe_3Nb_3X_x$ precipitates can also be important in 3D samples to prohibit grain boundary creep at high temperature.[4]

According to Figures 3 through 6, the volume fraction of the $Fe_3Nb_3X_x$ precipitates increases with time and temperature with a maximum below 1273 K (1000 °C). Between 1073 K and 1273 K (800 °C and 1000 °C) these precipitates form within 3 minutes, but not on the entire grain boundary. This seems in contradiction with the *in-situ* TEM experiments, where the sample was kept more than 1 hour above 1273 K to 1243 K (1000 °C to 970 °C) before the first nucleation of $Fe_3Nb_3X_x$ was observed. However, it is possible that nucleation effectively started below 1243 K (970 °C) but that it was not observed because it was outside the observation area. By increasing the holding time and observation area, the chance of observing the nucleation of $Fe_3Nb_3X_x$ at lower temperatures would increase. In the following Section IV–B the nucleation and growth of the $Fe_3Nb_3X_x$ precipitates during the *in-situ* TEM experiment will be discussed. This will be mainly focussed on the morphology shown in Figure 10, as this morphology is most frequently observed during postmortem analysis of the *in-situ* TEM samples.

B. *Nucleation and Growth Behavior of the* $Fe_3Nb_3X_x$ *Phase in the Presence of a* $Nb_2(C,N)$ *Precipitate*

From Figure 10, it can be seen that in the sample F1, the first $Fe_3Nb_3X_x$ precipitate nucleates at a distance from the $Nb_2(C,N)$ precipitate, which is in this case about 1.6 μm. The reason for this spacing between the initial $Nb_2(C,N)$ and the new $Fe_3Nb_3X_x$ precipitates originates from the production process. The condition of the sample at the beginning of the *in-situ* TEM experiment is the result of the last steps in the sheet production process, namely, hot rolling, annealing, and cooling. The temperature of the steel at the final hot rolling step is about 1173 K (900 °C). Annealing takes place at 1323 K (1050 °C). During cooling down, the steel attains all intermediate temperatures up to room temperature. Within the temperature range for which the $Nb_2(C,N)$ or $Nb(C,N)$ phases are stable for the given concentration Nb and (C,N) in the steel, $Nb_x(C,N)_y$ precipitates may form, but equilibrium will probably not be reached due to cinetic reasons. Only a local equilibrium at the $Nb_x(C,N)_y/\alpha$ (Fe,Cr) matrix interface can be assumed. Due to the relatively fast diffusion of C and N at this temperature, the concentration of C and N is likely homogeneous in the matrix and close to the equilibrium value at the interface between the precipitate and the matrix, assuming fast diffusion is not valid for the larger Nb atoms within the typical time scales of the production process. Far away from any $Nb_x(C,N)_y$

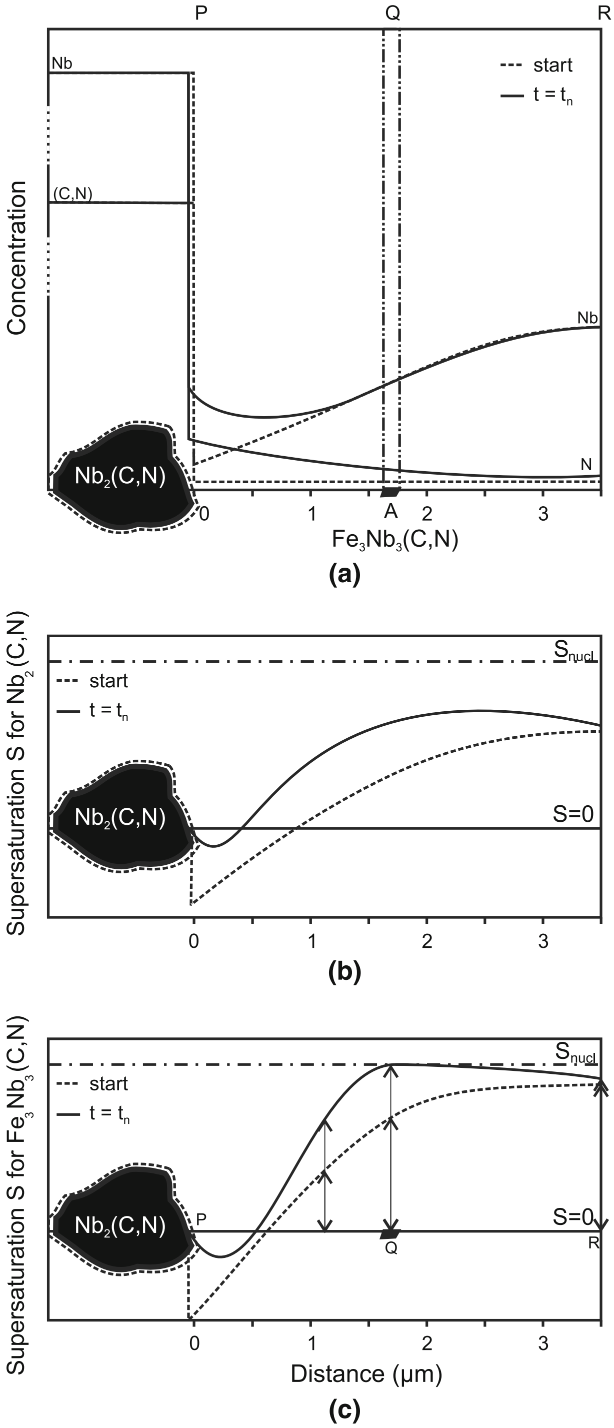

Fig. 14—(*a*) Concentration profiles of Nb and (C,N) around a $Nb_2(C,N)$ precipitate at the beginning of the *in-situ* TEM experiment (dashed lines) and at the moment t_n of the first nucleation of the $Fe_3Nb_3(C,N)$ phase after heating to 1243 K (970 °C) (solid lines). (*b*) and (*c*) Supersaturation in Nb and (C,N), respectively, for the $Nb_2(C,N)$ and $Fe_3Nb_3(C,N)$ phase.

precipitates, the concentration of Nb in the matrix is close to the global Nb concentration as only Nb atoms in the neighborhood of the $Nb_x(C,N)_y$ precipitate are consumed during the precipitation reaction. This gives a gradient in Nb concentration in the matrix, with a depletion of Nb around the $Nb_x(C,N)_y$ precipitates. The resulting concentration profiles of Nb and (C,N) around a $Nb_2(C,N)$ precipitate after the production process are visualized in Figure 14(a) by the dashed lines. To make an estimation of how large the depleted zone for Nb around a $Nb_2(C,N)$ precipitate is, the amount of Nb necessary to create the $Nb_2(C,N)$ can be expressed in the needed volume of the stainless steel matrix having 0.45 wt. pct Nb in solid solution. Assuming a spherical shape for the $Nb_2(C,N)$ in Figure 10 with a diameter of 1 μm and a linearly increasing Nb content from 0 to 0.45 wt. pct in the α (Fe,Cr) matrix, the depleted zone for Nb is a sphere with a radius of 3.2 μm. This is, however, only an approximation. First, the Nb concentration in the α (Fe,Cr) matrix at the $Nb_2(C,N)/\alpha$ (Fe,Cr) matrix interface will not be 0 but will have a finite value. Secondly, the Nb concentration in the Nb-depleted zone will not vary linearly, but rather with an error-function-like shape typical for diffusion processes. Therefore, the value of 3.2 μm for the radius of the depleted zone is a lower limit. As it is nonetheless the same order of magnitude as the observed distance between the $Nb_2(C,N)$ and $Fe_3Nb_3X_x$ precipitates, this depletion in Nb could be responsible for the spacing between the dissolving precipitate and the nucleating precipitates.

During the *in-situ* TEM experiment, the dissolution of the $Nb_2(C,N)$ precipitate appears limited up to 1243 K (970 °C) but at 1243 K (970 °C) the dissolution of $Nb_2(C,N)$ and the precipitation of $Fe_3Nb_3X_x$ are clearly observed. Through the dissolution of the $Nb_2(C,N)$ precipitate, the concentration profiles in the α (Fe,Cr) matrix around the $Nb_2(C,N)$ precipitate evolve from the dashed lines to the solid lines in Figure 14(a). The Nb atoms will concentrate mainly in the matrix next to the dissolving $Nb_2(C,N)$ precipitate due the low diffusion rate of Nb, thereby partially undoing the Nb depletion. The diffusion of the C and N atoms down the (C,N) chemical potential gradient towards the region with high Nb concentration will be much faster, especially along the grain boundary. As the nucleation of the $Fe_3Nb_3X_x$ precipitates at a grain boundary occurs only nearby a dissolving $Nb_2(C,N)$ precipitate, this reaction should be related to the diffusion of C and N. The $Fe_3Nb_3X_x$ phase, therefore, is assumed to be $Fe_3Nb_3(C,N)$[5–7] and not Fe_2Nb_3[4] or Fe_6Nb_6O.[7]

Nucleation of the $Fe_3Nb_3(C,N)$ phase will occur at this point where the supersaturation reaches the value S_{nucl}, either through an increase in Nb or in (C,N) concentration. A schematic representation of the supersaturation for the $Nb_2(C,N)$ and $Fe_3Nb_3(C,N)$ phase, which corresponds to the observations, is represented by the dashed lines in Figures 14(b) and (c). $S_{nucl}$is the supersaturation necessary for nucleation. As relatively more Nb atoms to (C,N) atoms are necessary to form the $Fe_3Nb_3(C,N)$ phase with up to 14 at. pct (C,N), Nb atoms are mainly come from the (Fe,Cr) matrix, while (C,N) atoms are mainly from the $Nb_2(C,N)$ precipitate.

In Figures 12 and 13, the growth of the precipitates A and C in the sample F1 was plotted. When only a few nuclei are present, the growth rate is high as (C,N) is readily available. During the initial nucleation and growth period, the diffusion of (C,N) will be the rate limiting factor as long as sufficient Nb is available around the $Fe_3Nb_3(C,N)$ precipitates. Along the grain boundary, precipitate A grows in the opposite direction of the diffusion of the (C,N) atoms. This explains its favored growth along this direction. This precipitate will consume a large part of the (C,N) atoms, leaving less for the other precipitates, which leads to the observed decrease in growth rate. After some time, the Nb depletion around the $Fe_3Nb_3(C,N)$ precipitates increased to the extent that the diffusion of Nb was the rate limiting step for further nucleation and growth.

A different precipitate morphology was observed in samples F2 where a $Fe_3Nb_3(C,N)$ nucleus appears to grow close to the $Nb_2(C,N)$ precipitate. The different configuration between sample F1 and F2 could be the reason. In F2, the $Nb_2(C,N)$ precipitate is initially not on the grain boundary, as in sample F1, but next to it (Figure 9). When the $Nb_2(C,N)$ begins to dissolve, C and N first have to diffuse through the matrix, which occurs at a slower rate than grain boundary diffusion. This leads to an increased concentration of (C,N) atoms around the $Nb_2(C,N)$ precipitate, thereby lowering the necessary concentration of Nb atoms to form $Fe_3Nb_3(C,N)$ nuclei. At the grain boundary close to the $Nb_2(C,N)$ precipitate, these nuclei are able to develop due to the supersaturation in Nb and (C,N) in combination with the grain boundary enhancing the diffusion of the elements towards the nuclei. The movement of the grain boundary caused the grain boundary to become the interface between the $Nb_2(C,N)$ precipitates and these $Fe_3Nb_3(C,N)$ nuclei.

V. CONCLUSIONS

The precipitation in Nb-stabilized Fe-15Cr-0.45Nb-0.010C-0.017N ferritic stainless steel with initial $Nb_2(C,N)$ precipitates is investigated with *in-situ* and *ex-situ* TEM. Both techniques give complementary data about the kinetics and morphology of newly formed $Fe_3Nb_3X_x$ precipitates. The following conclusions have been obtained:

1. $Fe_3Nb_3X_x$ precipitates are observed from 973 K to 1273 K (700 °C to 1000 °C) in *ex-situ* experiments. They form mainly at the grain boundary. Their volume fraction increases with time and temperature for up to at least 1173 K (900 °C). At 1273 K (1000 °C) the $Fe_3Nb_3X_x$ phase loses stability with respect to the $Nb_x(C,N)_y$ phase.
2. With *in-situ* TEM experiments, precipitation of $Fe_3Nb_3X_x$ is observed at 1243 K (970 °C). These experiments show that the precipitation of this phase is directly related to the dissolution of $Nb_2(C,N)$ precipitates at the grain boundary. The first $Fe_3Nb_3X_x$ precipitates will nucleate at a certain distance from a $Nb_2(C,N)$ precipitate due to the initial Nb depletion around these $Nb_2(C,N)$ precipitates.

This analysis indicates that C or N stabilizes the $Fe_3Nb_3X_x$ phase.

3. During and after the precipitate transition from the $Nb_2(C,N)$ to the $Fe_3Nb_3X_x$ precipitate, the grain boundary remains pinned by these precipitates.

ACKNOWLEDGEMENTS

One of the authors (AM) gratefully acknowledges the financial support of the Institute for the Promotion of Innovation through Science and Technology in Flanders (IWT-Vlaanderen). The authors thank the European Commission for the financial support through the Enabling Science and Technology through European Electron Microscopy (ESTEEM) project.

REFERENCES

1. N. Fujita, K. Ohmura, M. Kikuchi, T. Suzuki, S. Funaki, and I. Hiroshige: *Scripta Metall. Mater.*, 1996, vol. 35 (6), pp. 705–70.
2. A. Miyazaki, K. Takao, and O. Furukimi: *ISIJ Int.*, 2002, vol. 42 (8), pp. 916–20.
3. N. Fujita, K. Ohmura, and A. Yamamoto: *Mater. Sci. Eng. A*, 2003, vol. 351, pp. 272–81.
4. F. Chassagne, J.D. Mithieux, and J.H. Schmitt: *Steel Res. Int.*, 2006, vol. 77 (9-10), pp. 680–85.
5. G.M. Sim, J.C. Ahn, S.C. Hong, K.J. Lee, and K.S. Lee: *Mater. Sci. Eng. A*, 2005, vol. 396, pp. 159–65.
6. N. Fujita, M. Kikuchi, and K. Ohmura: *ISIJ Int.*, 2009, vol. 43 (12), pp. 1999–2006.
7. H. Holleck and F. Thümmler: *Mon. Chem.*, 1967, vol. 98, pp. 133–34.
8. F.X. Lü and K.H. Jack: *J. Less Common Met.*, 1985, vol. 114 (1), pp. 123–27.
9. N. Moelans, B. Blanpain, and P. Wollants: *Acta Mater.*, 2006, vol. 54 (4), pp. 1175–84.